

## Temperature Field and Thermal Deformation of Steel Structural Members in Construction Engineering



Jian Cheng

School of Resources and Environmental Engineering, Anhui Technical College of Water Resources and Hydroelectric Power, Hefei 231603, China

Corresponding Author Email: [chengjianzishan@163.com](mailto:chengjianzishan@163.com)

<https://doi.org/10.18280/ijht.400127>

### ABSTRACT

**Received:** 5 November 2021

**Accepted:** 17 January 2022

#### **Keywords:**

*construction engineering, steel structure, temperature field, thermal deformation*

The steel structure is increasingly applied in various building structures. It is of theoretical and practical significance to study the non-coordinated temperature field effects between the steel structure and external structure, and the strongly uneven temperature stress and marked deformation that ensue. However, the thermal boundary conditions are complex in the existing studies. Thus, this paper analyzes the temperature field and thermal deformation of steel structural members in construction engineering. Firstly, the relevant parameters were enumerated for the basic heat transfer modes, the temperature field of the steel members was calculated simply, and the convective heat transfer coefficients (CHTCs) of the members were discussed under different cross-sections and wind directions, presenting the accurate solution to thermal convection. Next, the thermal deformation of steel structural members was investigated to construct the thermal deformation equation of conventional steel structural members. Finally, experiments were carried out to compare the effects of different heat transfer parameters on the temperature stress of the components, and to summarize the entire process of building a thermal deformation equation for steel structure components.

## 1. INTRODUCTION

With the continuous upgrading of new building materials, construction engineering processes, and construction techniques, the steel structure is increasingly applied in various building structures, owing to its good ductility, strong plastic deformation capacity, and resistance to earthquakes and winds [1-8]. The commonly used building materials expand with heat and contract with cold. The steel structure is no exception: Different temperatures have different thermal stresses on the steel structure [9-15]. If there is an obvious construction defect, the steel structure will expand or shrink under sudden changes of the temperature [16-19]. Therefore, it is of theoretical and practical significance to study the non-coordinated temperature field effects between the steel structure and external structure. This issue has piqued the interest of the academia and engineering communities.

The construction process is crucial to large-span steel structures. To guide construction control, the construction process must be analyzed in the design stage. The structure force is influenced by complex load effects, the most important of which is the time-varying temperature field effect. Zhou et al. [20] proposed a new simulation method for the non-uniform time-varying temperature field of large-span steel structures, which computes the shadow effect and the actual solar radiation absorbed by tubular members. The proposed method was combined with the construction process simulation to accurately emulate the temperature effect during the construction process. To clarify the process of the steel structure from damage accumulation to failure under extreme cyclic load and temperature, Guo et al. [21] established a

multi-scale fatigue-creep injury model, and constructed a multi-scale fatigue damage model by the generalized self-consistent method, drawing on the microcrack density equilibrium theory. Shnal et al. [22] proposed a mathematical model to disclose the effects of fire temperature state on the structural mechanical properties of the metallic structure, plotted a monogram for the fire resistance limit of the steel structure under critical temperature standard, and developed an appropriate approach. Based on the theory of heat transfer, Qiu et al. [23] studied the similarity theory on the temperature field of light steel members under fire, presented a simplified furnace temperature curve, and verified the curve both numerically and experimentally. In addition, they compared the influencing factors of the similarity theory on the temperature field of light steel members with or without intumescent fire-retardant coatings.

The existing thermodynamic theoretical analyses and finite-element thermal analyses involve complex thermal boundaries, and cannot fully monitor the various temperature boundary conditions. To further explore the law of complex environmental factors acting on the temperature field and thermal deformation of the steel structure, this paper discusses the heat transfer modes of steel structural members. The main contents cover the following aspects: Section 2 enumerates the relevant parameters for the basic heat transfer modes, completes the simplified calculation of the temperature field of the steel members, and discusses the convective heat transfer coefficients (CHTCs) of the members under different cross-sections and wind directions, presenting the accurate solution to thermal convection. Section 3 investigates the thermal deformation of steel structural members, and

constructs the thermal deformation equation of conventional steel structural members. Finally, experiments were carried out to compare the effects of different heat transfer parameters on the temperature stress of the components, and to summarize the entire process of building a thermal deformation equation for steel structure components.

## 2. TEMPERATURE FIELD ANALYSIS

In construction engineering, the heat exchange between exposed steel structural members and the outside world never stops. The overall temperature field distribution depends on three basic heat transfer modes: the thermal conduction, convection, and radiation between the sun, the air, and the ground. Figure 1 lists the parameters of the basic heat transfer modes.

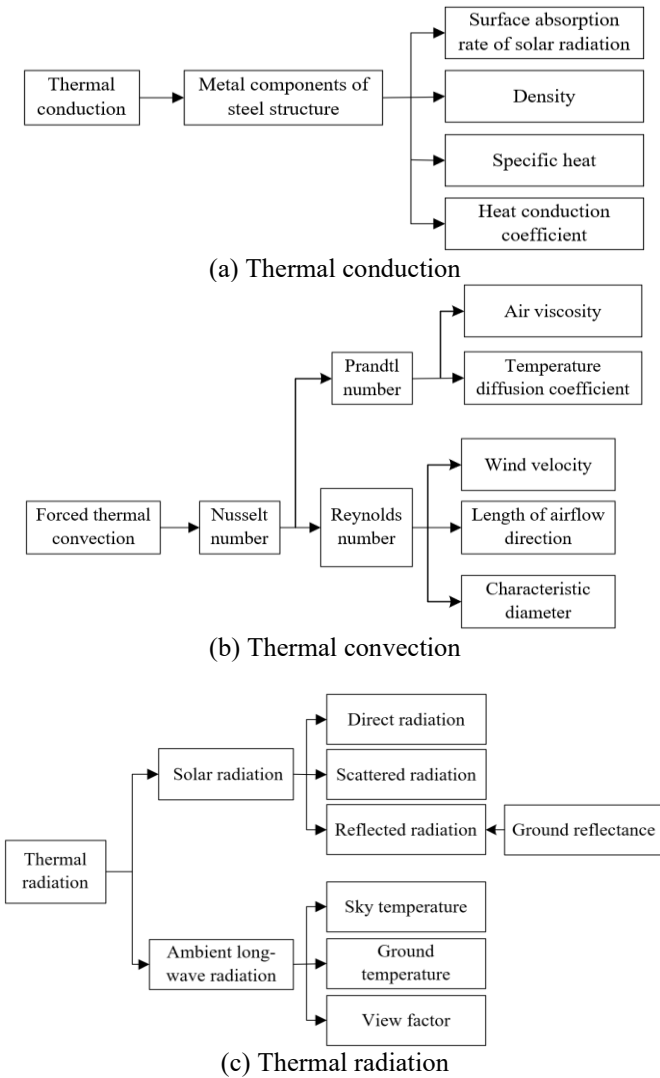


**Figure 1.** Parameters of basic heat transfer modes

Suppose the outer interface of a steel structural member is in a thermal equilibrium state, that is, neither heat transfer nor material phase change occurs on the interface between the member and the outside, and the temperature state is uniform across the interface. Based on the basic principle of thermodynamics, the heat radiated from the interface of the member equals the heat transferred from the inside of the member to the interface. Let  $HT_R$  be the heat transferred by the

thermal conduction of the steel structural member itself;  $HT_S$  be the heat transferred by the radiation between the member surface and the sun;  $HT_D$  be the heat transferred by the thermal convection between the member surface and the surrounding air;  $HT_A$  be the heat transferred by the long-wave radiation between the member surface and the sky;  $HT_W$  be the heat transferred by the long-wave radiation between the member surface and the ground. Then, the thermal equilibrium of the steel structural member can be expressed as:

$$HT_R = HT_S + HT_D + HT_A + HT_W \quad (1)$$

Let  $\beta_1$  and  $\beta_2$  be the radiation absorption rates of the sky and the ground, respectively;  $\Phi_1$  and  $\Phi_2$  be the radiant surface areas of the sky and the ground, respectively;  $\omega_1$  and  $\omega_2$  be the view factors of the sky and the ground, respectively;  $\rho$  be the surface absorption rate of solar radiation of the steel structural member;  $\Phi_G$  be the surface area of the member receiving solar radiation;  $TS$  be the total strength of solar radiation on the member surface;  $\sigma$  be the unit radiation reflectance of the member surface;  $\varepsilon$  be the Stefan-Boltzmann constant;  $\gamma$  be the absolute temperature of the member surface;  $\gamma_D$ ,  $\gamma_A$ , and  $\gamma_W$  be the temperature of the air, the sky, and the ground, respectively. The thermal equilibrium of the steel structural member can be expressed as:

$$-l\Phi_R \frac{\partial \gamma}{\partial a} = -\rho\Phi_G TS + f_D\Phi_D(\gamma - \gamma_D) + \sigma\beta_1\varepsilon\Phi_1\omega_1(\gamma^4 - \gamma_A^4) + \sigma\beta_2\varepsilon\Phi_2\omega_2(\gamma^4 - \gamma_W^4) \quad (2)$$

The maximum temperature generally appears at the top of the steel structural member. Thus, it is assumed that the temperature distribution is uniform in the thickness direction of the top of the member. That is, the heat from the inside to the top interface of the member is approximately zero. Then, we have:

$$HT_R = -l\Phi_R \frac{\partial \gamma}{\partial a} \approx 0 \quad (3)$$

$$-\rho\Phi_G TS + f_D\Phi_D(\gamma - \gamma_D) + \sigma\beta_1\varepsilon\Phi_1\omega_1(\gamma^4 - \gamma_A^4) + \sigma\beta_2\varepsilon\Phi_2\omega_2(\gamma^4 - \gamma_W^4) = 0 \quad (4)$$

Let  $(\cos \alpha, \sin \alpha)$  be the unit normal vector representing the spatial orientation of the member;  $f_D$  be the CHTC between the member and the surrounding air. The values of  $\Phi_G$ ,  $\Phi_D$ ,  $\Phi_1$ , and  $\Phi_2$  are set as equal, and  $\sigma$ ,  $\beta_1$ , and  $\beta_2$  are set to 0.8, 0.8, and 0.6, respectively. Then, we have:

$$-\rho TS + f_D(\gamma - \gamma_D) + 1.79 \times 10^{-8}(1 + \sin \alpha)(\gamma^4 - \gamma_A^4) + 1.34 \times 10^{-8}(1 - \sin \alpha)(\gamma^4 - \gamma_W^4) = 0 \quad (5)$$

$$-\rho TS + f_D(\gamma - \gamma_D) + 3.68 \times 10^{-8}(1 + 0.15 \sin \alpha)T^4 - 1.79 \times 10^{-8}(1 + \sin \alpha)\gamma_A^4 - 1.33 \times 10^{-8}(1 - \sin \alpha)\gamma_W^4 = 0 \quad (6)$$

By introducing the sky and ground temperatures, we have:

$$-\rho TS + f_D(\gamma - \gamma_D) + 3.68 \times 10^{-8}(1 + 0.15 \sin \alpha)\gamma^4 - 1.72 \times 10^{-13}(1 + \sin \alpha)\gamma_D^6 - 1.32 \times 10^{-8}(1 - \sin \alpha)(\gamma_D + 8)^4 = 0 \quad (7)$$

Considering the actual physical meaning of each variable, and the regional difference in the maximum temperature, the high-order terms in the above formula are simplified in the highest temperature range, producing the following linear fitting formula:

$$\begin{aligned} &-\rho TS + f_D(\gamma - \gamma_D) + (1 + 0.15\sin\alpha)(4.24\gamma - 1028) \\ &-(1 + \sin\alpha)(2.34\gamma_D - 771) \\ &-(1 - \sin\alpha)(1.68\gamma_D - 327) = 0 \end{aligned} \quad (8)$$

$$\begin{aligned} &-\rho TS + (f_D + 0.55\sin\alpha + 4.31)\gamma \\ &-(f_D + 0.99\sin\alpha + 4.45)\gamma_D + 165\sin\alpha + 77 = 0 \end{aligned} \quad (9)$$

The surface temperature of the steel structural member can be calculated by:

$$\gamma = \frac{\rho TS + (f_D + 0.99\sin\alpha + 4.45)\gamma_D - 165\sin\alpha - 77}{f_D + 0.55\sin\alpha + 4.31} \quad (10)$$

Converting the temperature unit of formula (10) from K to °C, we have:

$$\gamma = \frac{\rho TS + (f_D + 0.99\sin\alpha + 4.45)(\gamma_D + 273.15) - 273.15f_D - 322\sin\alpha - 1188}{f_D + 0.55\sin\alpha + 4.31} \quad (11)$$

The above analysis shows that the surface temperature of the steel structural member is closely associated with  $\rho$ ,  $TS$ ,  $f_D$ ,  $\gamma_D$ , and  $\alpha$ . The sensitivity coefficients of the relevant parameters are listed in Table 1.

During the temperature field analysis on the exposed structural members the construction engineering, the precise solution of thermal convection requires a thorough discussion on the CHTCs of the members at different cross-sections and wind directions. The thermal convection takes two forms: the forced thermal convection driven by power or pressure, and the natural thermal convection induced by density. The latter form is included in the former. For simplicity, the influence of the latter is so small as to be negligible.

In forced thermal convection, it is difficult to analyze the thermal fluid from the angles of fluidity and dynamics. The key parameter of CHTC computing is the Nusselt number, which involves the Prandtl number and Reynolds number. When the fluid passes the plate in a random direction, the CHTC can be calculated by:

$$f_k = \frac{M\lambda_k \times l}{K} \quad (12)$$

**Table 1.** Sensitivity coefficients of relevant parameters

Relevant parameters		Highest temperature	Lowest temperature
$(\cos \alpha, \sin \alpha)$	Horizontal	-0.015	-0.025
	Vertical	-0.042	-0.042
	$\rho$	0.362	0.249
	$TS$	0.216	0.024
	$\gamma_D$	0.517	0.815
	$v$	-0.061	-0.037
	$\sigma$	0.027	0.029

When the fluid passes the axial direction of the tubular member vertically, the CHTC can be calculated by:

$$f_p = \frac{M\mu_p \times l}{P} \quad (13)$$

Let  $\zeta$  be the Prandtl number;  $\nu$  be the kinematic viscosity;  $\beta$  be the temperature diffusion coefficient;  $SH_\chi$  be the specific heat capacity of the fluid;  $\lambda$  be the absolute viscosity;  $\chi$  be the air density at different altitudes;  $l$  be the thermal conductivity coefficient of the air. Then, we have:

$$\zeta = \nu / \beta \quad (14)$$

$$\nu = \lambda / \chi \quad (15)$$

$$\beta = l / \chi SH_\chi \quad (16)$$

Let  $v$  be wind velocity. For a plate with the length of  $H$  along the airflow direction, the Reynolds number can be calculated by:

$$LN_H = vH / \nu = vH\chi / \lambda \quad (17)$$

For a tubular member with a diameter of  $R$ , and an axis vertical to the airflow direction, the Reynolds number can be calculated by:

$$LN_R = vR / \nu = vR\chi / \lambda \quad (18)$$

During the calculation of Reynolds number, the characteristic diameter  $R_f$  of the cross-section of the special steel structural member is roughly four times the hydraulic radius  $R_w$ . Table 2 presents the sensitivity coefficients of relevant parameters for steel structural members with different cross-sections. Note that  $x$  and  $y$  are the long side length and short side length of the cross-section, respectively;  $g$  is the wall thickness. For a non-ventilated rectangular steel tube with two closed ends, the hydraulic radius  $R_w$  of any member can be calculated by:

$$R_w = \frac{xy}{2(x+y)} \quad (19)$$

For a ventilated rectangular steel tube with two open ends, the hydraulic radius  $R_w$  of any member can be calculated by:

$$R_w = \frac{[xy + (x-2g)(y-2g)]}{2(x+y)2(x-2g+y-2g)} \quad (20)$$

Let  $x$  and  $y$  be width and height, respectively;  $g_1$  and  $g_2$  be the thicknesses of the flange and the web, respectively. For an H-steel structure, the hydraulic radius  $R_w$  can be calculated by:

$$R_w = \frac{[2xg_1 + (y-2g_1)g_2]}{4(x+g_1) + 2(y-2g_1+g_2)} \quad (21)$$

Let  $R$  and  $g$  be diameter and wall thickness, respectively. For a ventilated circular steel tube with two open ends, the hydraulic radius  $R_w$  of any member can be calculated by:

**Table 2.** Sensitivity coefficients of relevant parameters for steel structural members with different cross-sections

Building type and interface parameter		Highest temperature	Lowest temperature
Rectangular tube	$x$	0.049	-0.084
	$y$	0.261	0.017
	$g$	-0.062	0.085
	$x$	-0.013	-0.037
H-steel	$y$	0.185	-0.016
	$g_1$	-0.038	0.041
	$g_2$	-0.046	0.062
Circular tube	$R$	0.137	-0.115
	$g$	-0.027	0.039

$$R_w = \frac{\pi R^2 / 4 - \pi (R - 2g)^2 / 4}{\pi (R + R - 2g)} \quad (22)$$

The mean Nusselt number of flat plate laminar flow can be calculated by:

$$NS_H = 0.67 \times \sqrt[2]{LN_H} \times \sqrt[3]{PR} \quad (23)$$

The mean Nusselt number of turbulent flow can be calculated by:

$$NS_H = 0.04 \times 1.25 \sqrt[2]{LN_H} \times \sqrt[3]{PR} \quad (24)$$

When the wind direction is perpendicular to the axis of the circular steel tube, the mean Nusselt number of a single circular tube can be calculated by:

$$NS_R = 0.33 \times \sqrt[1.75]{LN_R} \quad (25)$$

The mean Nusselt number of multiple circular tubes can be calculated by:

$$NS_{mR} = 0.33 \times 1.66 \sqrt[1.66]{LN_R} \times \sqrt[3]{PR} \quad (26)$$

### 3. THERMAL DEFORMATION ANALYSIS

It is assumed that the chemical composition of the metallic material of the steel structural member does not change. Let  $\rho$  be the deformation rate;  $\varepsilon_{CV}$  be the peak stress;  $EW$  be the dynamic recrystallization activation energy;  $DW$  be the deformation temperature;  $GC$  be the gas constant;  $X$ ,  $\beta$ , and  $\eta$  be the relevant test parameters. Then, the relationship between the strain rate, the deformation temperature, and the peak stress satisfies the double-sinusoidal equation:

$$\rho = X [\sinh(\beta \varepsilon_{CV})]^\eta \exp\left(-\frac{EW}{GC \cdot DW}\right) \quad (27)$$

If  $\beta \varepsilon < 0.5$ , i.e., the stress is low, formula (27) can be simplified as:

$$\rho = X_1 \varepsilon^\eta \exp\left(-\frac{EW}{GC \cdot DW}\right) \quad (28)$$

Suppose  $\beta$ ,  $\phi$ , and  $\eta_k$  satisfy  $x = \phi / \eta_k$ . If  $\beta \varepsilon > 0.5$ , i.e., the stress

is high, formula (27) can be simplified as:

$$\rho = X_2 \exp(\varphi \varepsilon) \left(-\frac{EW}{GC \cdot DW}\right) \quad (29)$$

Taking the natural logarithm and partial derivative on the left and right sides of formula (29), respectively, we have:

$$\eta_i = \left[ \frac{\partial \ln \rho}{\partial \ln \varepsilon} \right]_T \quad (30)$$

$$\varphi = \left[ \frac{\partial \ln \rho}{\partial \ln \varepsilon} \right]_T \quad (31)$$

Taking the natural logarithm of formula (27), we have:

$$\ln[\sinh(\beta \varepsilon_{CV})] = \frac{1}{\eta} \ln \rho + \frac{EW}{\eta \cdot GC \cdot DW} - \frac{1}{\eta} \ln X \quad (32)$$

Taking the partial derivative of deformation rate on both sides of formula (32), we have:

$$\frac{1}{\rho} = \left[ \frac{\partial \ln \sinh(\beta \varepsilon_{CV})}{\partial \ln \rho} \right]_T \quad (33)$$

Taking the partial derivative of  $1/DW$  on both sides of formula (32), the thermal deformation activation energy can be calculated by:

$$EW = \eta \cdot GC \left[ \frac{\partial \ln \sinh(\beta \varepsilon_{CV})}{\partial (1/DW)} \right]_T \quad (34)$$

The thermal deformation equation for conventional steel structural members can be expressed as:

$$\rho = 1.5 \times 10^{16} [\sinh(6 \times 10^{-3} \varepsilon)]^7 \exp\left(-\frac{4.2 \times 10^5}{GC \cdot DW}\right) \quad (35)$$

The overall action of  $\rho$  and  $DW$  on the thermal deformation of the steel structural member can be characterized by the Zener–Hollomon (ZH) parameter:

$$ZH = \rho \exp\left(\frac{EW}{GC \cdot DW}\right) \quad (36)$$

Combining formula (36) and formula (27), we have:

$$ZH = X [\sinh(\beta \varepsilon_{CV})]^\eta \quad (37)$$

Taking the natural logarithm on both sides of formula (37), we have:

$$\ln ZH = \ln X + \eta \ln [\sinh(\beta \varepsilon)] \quad (38)$$

Based on the  $W$  value obtained by formula (34), it is possible to derive the  $ZH$  value under different deformation conditions of the steel structure. The  $\ln[\sinh(\beta \varepsilon_{CV})]$  has a linear relationship with  $\ln ZH$ . With the growth of  $ZH$ , the  $\varepsilon_{CV}$  will increase through the thermal deformation of the steel structural member. The correlation coefficient between the two parameters is close to 0.99.

#### 4. EXPERIMENTS AND RESULTS ANALYSIS

Figure 2 displays the influence of different heat transfer parameters on temperature stress of the steel structural member, including solar radiation strength  $TS$ , air temperature  $\gamma_D$ , wind velocity  $v$ , and absorption rate of solar radiation  $\sigma$ . It can be seen that the  $TS$  had a prominent effect on the axial and

bending thermal stresses of the steel structural member. Both stresses are positively proportional to  $TS$ . Every 100  $W/m^2$  increment of  $TS$  pushed up the axial and bending thermal stresses by 3 MPa and 0.8 MPa, respectively. Hence, the steel structural member has better overall thermal stress in good weather than in bad weather.

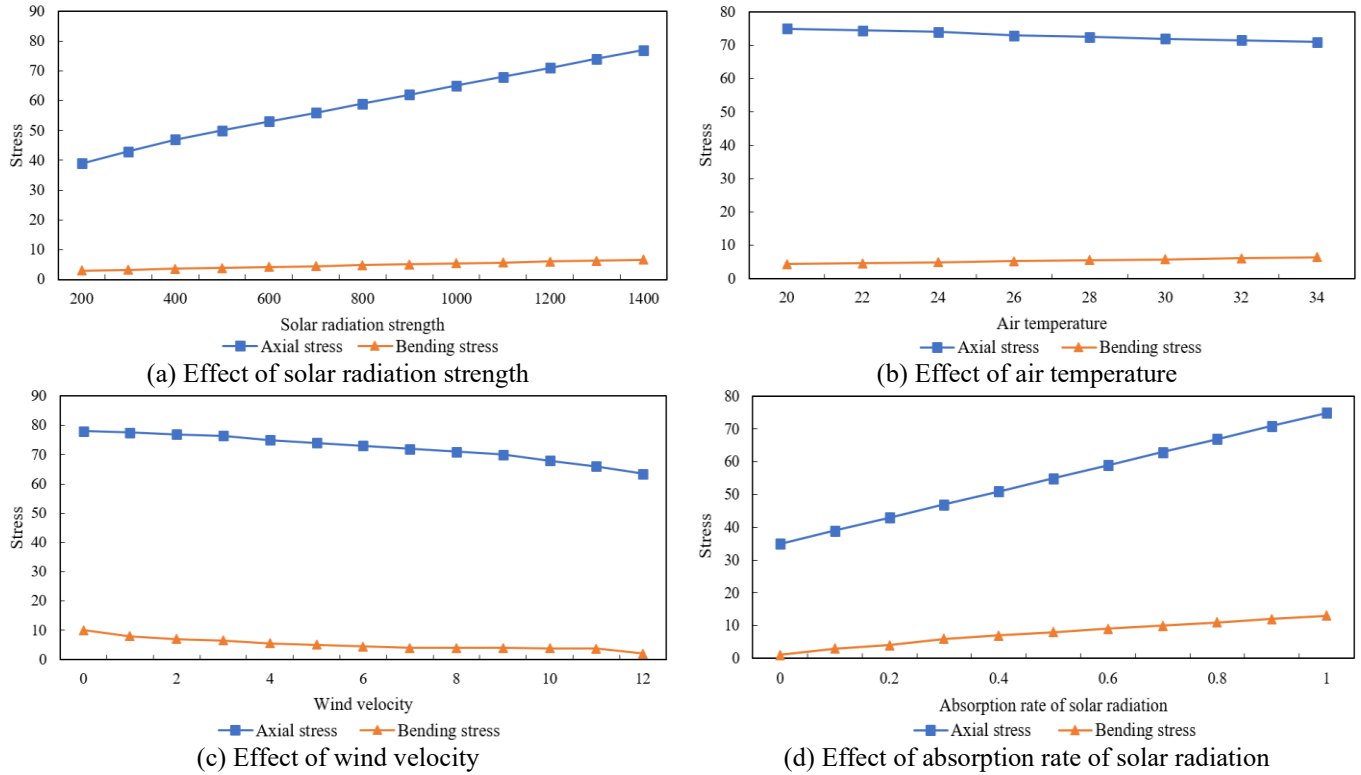


Figure 2. Influence of different heat transfer parameters on temperature stress of the steel structural member

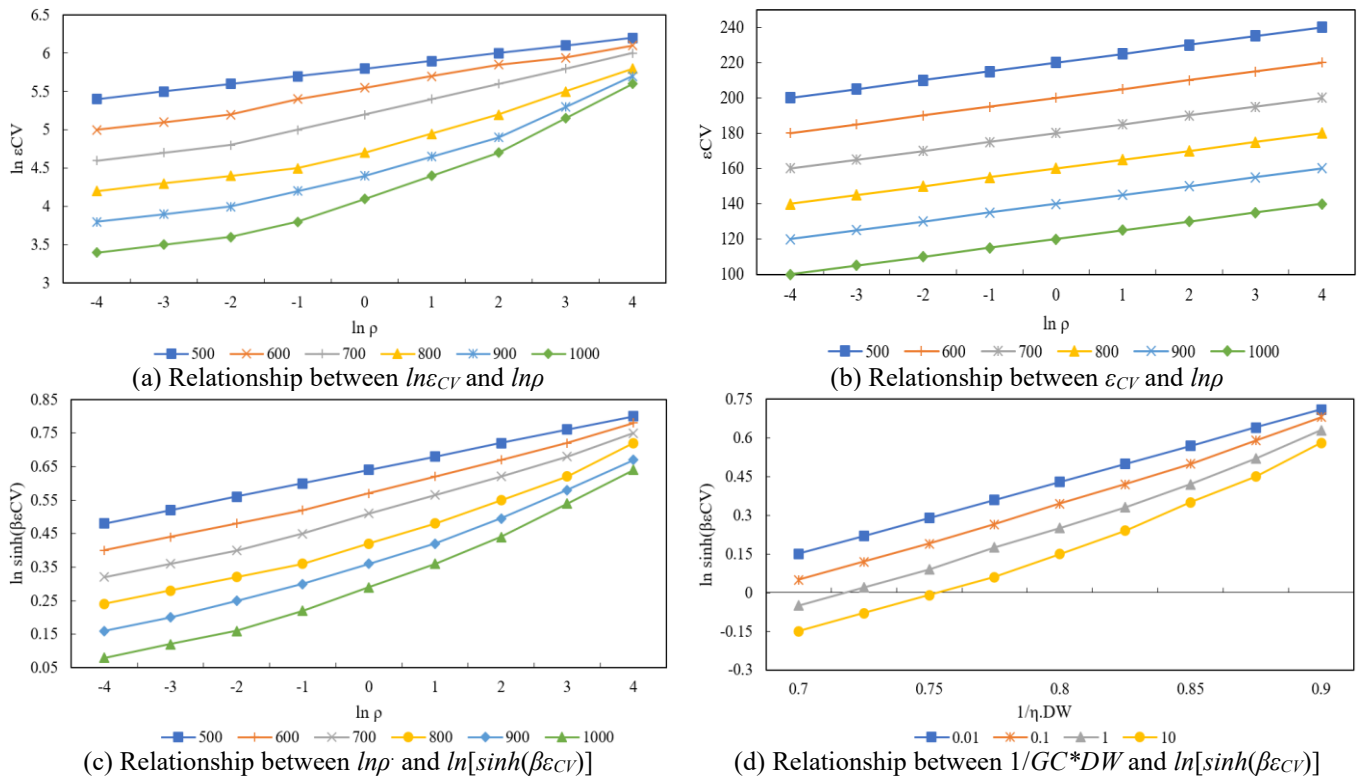


Figure 3. Interpolation curves under different deformation conditions of the steel structural member

Besides,  $\gamma_D$  had a relatively obvious influence on the axial thermal stress of the steel structural member. Every 1°C increment of  $\gamma_D$  pushed up the axial stress by 1.5 MPa. Meanwhile,  $\gamma_D$  had a relatively small impact on the bending stress.

When  $v$  was slower than 5m/s, it exerted the greatest impact on the axial thermal stress of the member. Every 1m/s increment of the wind velocity dragged down the axial stress by 9.8 MPa. When  $v$  was greater than 5m/s, it had a small impact on the axial stress of the member. Every 1m/s increment of the wind velocity only reduced the axial stress by 1.8 MPa. When  $v$  was greater than 10m/s, the axial thermal temperature changed no more. In this case, the wind velocity had a small effect, and exhibited a nearly negative correlation with the axial pressure. Every 1m/s increment of the wind velocity merely lowered the axial stress by 0.25 MPa. Hence, the temperature effect on the steel structural member is insignificant if the member is well ventilated.

In addition,  $\sigma$  is positively proportional to the axial and bending thermal stresses of the member. Every 0.1 increment of  $\sigma$  pushed up the axial and bending stresses by 4.7 MPa and 1.4 MPa, respectively. Thus, the  $\sigma$  of the surface coating of the member must be fully considered to compute the temperature effect more accurately.

Figure 3 displays the interpolation curves under different deformation conditions of the steel structural member. The relationship between  $\ln \varepsilon_{CV}$  and  $\ln \rho$  is shown in Figure 3(a). The reciprocal of the slope can be solved as 9.2133 according to the fitted curve. The relationship between  $\varepsilon_{CV}$  and  $\ln \rho$  is shown in Figure 3(b). The  $\phi$  value can be solved as 0.0447 according to the fitted curve. Based on  $\eta_k$  and  $\phi$ , it can be further computed that  $x = \phi/m_k = 0.00485$ . The relationship between  $\ln \rho$  and  $\ln[\sinh(\beta \varepsilon_{CV})]$  is shown in Figure 3(c). Through linear regression, the test parameter  $\eta$  can be solved as 6.9. The relationship between  $1/GC * DW$  and  $\ln[\sinh(\beta \varepsilon_{CV})]$  is shown in Figure 3(d). The thermal deformation activation energy  $EW$  can be solved as 398.661  $kJ/mol$ , according to the fitted curve. Finally, the test parameter  $X$  can be solved as  $1.41 \times 10^{16}$ , referring to the intercept of the steel structural member. From all the parameters above, it is possible to construct the thermal deformation equation for the member.

The relationship between  $\ln[\sinh(\beta \varepsilon_{CV})]$  and  $\ln ZH$  is given in Figure 4. It can be seen that  $\ln[\sinh(\beta \varepsilon_{CV})]$  is linearly correlated with  $\ln ZH$ , which agrees with the theoretical analysis. The figure visually displays that  $\varepsilon_{CV}$  increases with  $ZH$  during the thermal deformation of the steel structural member.

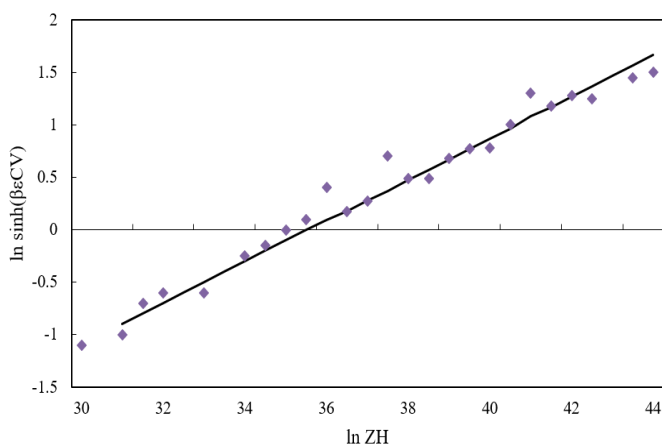


Figure 4. Relationship between  $\ln[\sinh(\beta \varepsilon_{CV})]$  and  $\ln ZH$

## 5. CONCLUSIONS

This paper investigates the temperature field and thermal deformation of steel structural members in construction engineering. Firstly, the authors summarized the relevant parameters for the basic heat transfer modes, completed simplified calculation of the temperature field of the steel members, and discussed the CHTCs of the members were discussed under different cross-sections and wind directions. In this way, the thermal convection was solved accurately. On this basis, the authors investigated the thermal deformation of steel structural members, and constructed the thermal deformation equation of conventional steel structural members. Through experiments, the authors examined the influence of different heat transfer parameters over the thermal stress of the member, including solar radiation strength  $TS$ , air temperature  $\gamma_D$ , wind velocity  $v$ , and absorption rate of solar radiation  $\sigma$ . Based on the experimental results, several suggestions were provided for steel structure design. In addition, the interpolation curves were plotted for the deformation of steel structural members, and the steps of building the thermal deformation equation for the members were detailed. Finally, the relationship between  $\ln[\sinh(\beta \varepsilon_{CV})]$  and  $\ln ZH$  was drawn, and the variation of the relevant parameters was discussed during the thermal deformation of the said members.

## REFERENCES

- [1] Morelli, F., Piscini, A., Salvatore, W. (2017). Seismic behavior of an industrial steel structure retrofitted with self-centering hysteretic dampers. *Journal of Constructional Steel Research*, 139: 157-175. <https://doi.org/10.1016/j.jcsr.2017.09.025>
- [2] Shlyakhova, G.V., Barannikova, S.A., Bochkareva, A.V., Li, Y.V., Zuev, L.B. (2018). Structure of a carbon steel-stainless steel bimetal. *Steel in Translation*, 48(4): 219-223. <https://doi.org/10.3103/S0967091218040101>
- [3] Du, N.J., Bai, G.L., Liu, L., Zhao, X.G. (2017). Experimental study and analysis on hysteretic behavior of steel-concrete hybrid air-cooling structure with steel braces. *Engineering Mechanics*, 34(5): 205-215.
- [4] Nikitina, E.N., Glezer, A.M., Ivanov, Y.F., Aksenova, K.V., Gromov, V.E., Kazimirov, S.A. (2017). Evolution of the structure and the phase composition of a bainitic structural steel during plastic deformation. *Russian Metallurgy (Metally)*, 2017(10): 871-873. <https://doi.org/10.1134/S0036029517100159>
- [5] Zajec, B., Bajt Leban, M., Kosec, T., et al. (2018). Corrosion monitoring of steel structure coating degradation. *Tehnički Vjesnik*, 25(5): 1348-1355. <https://doi.org/10.17559/TV-20170206004112>
- [6] Xu, L.H., Xiao, S.J., Wu, Y.W., Li, Z.X. (2018). Seismic failure mode identification and multi-objective optimization for steel frame structure. *Advances in Structural Engineering*, 21(13): 2005-2017. <https://doi.org/10.1177%2F1369433218764619>
- [7] Yan, J.B., Liu, X.M., Liew, J.R., Qian, X., Zhang, M. H. (2016). Steel-concrete-steel sandwich system in Arctic offshore structure: Materials, experiments, and design. *Materials & Design*, 91: 111-121. <https://doi.org/10.1016/j.matdes.2015.11.084>
- [8] Yan, J.B., Liew, J.R., Zhang, M.H., Li, Z.X. (2016). Punching shear resistance of steel-concrete-steel

- sandwich composite shell structure. *Engineering Structures*, 117: 470-485. <https://doi.org/10.1016/j.engstruct.2016.03.029>
- [9] Xie, Z., Zhang, J., Mei, G., Zhao, S., Liang, B., Lin, Y. (2014). A novel structure of blackbody cavity sensor for continuous measurement of molten steel temperature. *ISIJ International*, 54(8): 1849-1855. <https://doi.org/10.2355/isijinternational.54.1849>
- [10] Stratulat, A., Duff, J.A., Marrow, T.J. (2014). Grain boundary structure and intergranular stress corrosion crack initiation in high temperature water of a thermally sensitised austenitic stainless steel, observed in situ. *Corrosion Science*, 85: 428-435. <https://doi.org/10.1016/j.corsci.2014.04.050>
- [11] Duan, W. Z., Li, L., Han, J. P., Zhou, J., Xiang, C. S. (2013). Construction method of low temperature welding for large-span steel truss beam structure. *Advanced Materials Research*, 671: 2025-2028. <https://doi.org/10.4028/www.scientific.net/AMR.671-674.2025>
- [12] Kariya, T., Tanaka, H., Hirono, T., et al., (2016). Development of a novel cell structure for low-temperature SOFC using porous stainless steel support combined with hydrogen permeable Pd layer and thin film proton conductor. *Journal of Alloys and Compounds*, 654: 171-175. <https://doi.org/10.1016/j.jallcom.2015.09.109>
- [13] Koptseva, N.V., Efimova, Y., Nikitenko, O.A., Baryshnikov, M.P., Zhrebtsov, M.S. (2016). Formation of ultrafine-grain structure in carbon steel by high-temperature high-speed compression. *Steel in Translation*, 46(2): 103-106. <https://doi.org/10.3103/S0967091216020066>
- [14] Churyumov, A.Y., Khomutov, M.G., Tsar'kov, A.A., Pozdnyakov, A.V., Solonin, A.N., Mukhanov, E.L. (2015). Boron-containing steel structure and properties at room and elevated temperature. *Metallurgist*, 58(11): 992-997. <https://doi.org/10.1007/s11015-015-0029-1>
- [15] Stepanov, A.I., Ashikhmina, I.N., Sergeeva, K.I., Belikov, S.V., Musikhin, S. A., Karabanalov, M.S., Al-Katawi, A.A. (2014). Structure and properties of low-alloy Cr-Mo-V steel after austenitization in the intercritical temperature range. *Steel in Translation*, 44(6): 469-473. <https://doi.org/10.3103/S0967091214060151>
- [16] Luo, Y., Mei, Y.J., Shen, Y.B., Yang, P.C., Jin, L., Zhang, P.F. (2013). Field measurement of temperature and stress on steel structure of the National Stadium and analysis of temperature action. *Jianzhu Jieqou Xuebao/Journal of Building Structures*, 34(11): 24-32.
- [17] Dai, S.J., Lv, C., Chen, Q. (2013). Calculation and analysis of temperature stress for large-span steel structure. *Applied Mechanics and Materials*, 405: 944-947. <https://doi.org/10.4028/www.scientific.net/AMM.405-408.944>
- [18] Craveiro, H.D., Rodrigues, J.P.C., Santiago, A., Lafm, L. (2016). Review of the high temperature mechanical and thermal properties of the steels used in cold formed steel structures—The case of the S280 Gd+ Z steel. *Thin-Walled Structures*, 98: 154-168. <https://doi.org/10.1016/j.tws.2015.06.002>
- [19] Lambrakos, S.G. (2016). Temperature histories of structural steel welds calculated using solidification-boundary constraints. *Journal of Materials Engineering and Performance*, 25(9): 4070-4080. <https://doi.org/10.1007/s11665-016-2243-9>
- [20] Zhou, M., Fan, J.S., Liu, Y.F., Zhang, J.X., Duan, X.J., Lei, S.S. (2020). Non-uniform temperature field and effect on construction of large-span steel structures. *Automation in Construction*, 119: 103339. <https://doi.org/10.1016/j.autcon.2020.103339>
- [21] Guo, H., Sun, B., Li, Z. (2020). A multi-scale fatigue-creep coupled damage model for steel structures under extreme cyclic loading and temperature. *International Journal of Damage Mechanics*, 29(4): 591-609. <https://doi.org/10.1177/1056789519871339>
- [22] Shnal, T., Pozdieiev, S., Nuianzin, O., Sidnei, S. (2020). Improvement of the assessment method for fire resistance of steel structures in the temperature regime of fire under realistic conditions. *Materials Science Forum*, 1006: 107-116. <https://doi.org/10.4028/www.scientific.net/MSF.1006.107>
- [23] Qiu, C.H., Zhang, G.Y., Li, B.Y., Tong, Y., Liu, Q., Wang, G.Y. (2020). Research on the similarity theory of temperature field of light steel members (structures) under fire. *Gongcheng Lixue/Engineering Mechanics*, 37(11): 176-184. <https://doi.org/10.6052/j.issn.1000-4750.2020.01.0009>